EnvironmentAsia
The international journal by the Thai Society of Higher Education Institutes on Environment

EnvironmentAsia 17(2) 2024 127-144
DOI 10.14456/ea.2024.26
ISSN 1906-1714; ONLINE ISSN: 2586-8861

Defluoridation from Aqueous Solutions Using Activated Cow Bone

Yanasinee Suma[1], Numfon Eaktasang[2], and Pradabduang Kiattisaksiri[1*]

[1] *Faculty of Public Health, Thammasat University (Lampang campus), Lampang, Thailand*
[2] *Faculty of Public Health, Thammasat University (Rangsit campus), Pathumthani, Thailand*

*Corresponding author: Pradabduang.k@fph.tu.ac.th
Received: September 18, 2023; Revised: October 13, 2023; Accepted: January 26, 2024

Abstract

The objective of this study was to synthesize activated carbon from cow bones (ACB). The investigation focused on identifying the optimal synthesis conditions for ACB and subsequently evaluating its efficacy in adsorbing fluoride in synthetic and natural groundwater samples. The findings revealed that pyrolyzing cow bones at 600 ºC for 1 h exhibited superior fluoride adsorption capabilities (6 mg/L) in synthetic water compared to pyrolysis at 400 and 500 ºC, attributed to the largest surface area (144.20 m^2/g). The highest observed fluoride adsorption efficiency reached 85.87 ± 2.78% within 15 min. The optimal dosage and particle size of the ACB were determined to be 0.5 g and within the range of 30 - 50 mesh, respectively. Additionally, the study demonstrated that fluoride adsorption efficiency was notably enhanced at pH 5 compared to pH 7 and 9, exhibiting an upward trend with increasing fluoride concentration. The maximum adsorption capacity of the ACB was 0.52 mg/g. The adsorption isotherms of fluoride matched well with the Langmuir isotherm model (R^2 = 1.000) and the pseudo-second-order kinetic (R^2 = 0.9969). In evaluations conducted with natural groundwater, the ACB achieved a successful adsorption rate of approximately 74.95 ± 7.38% for an initial fluoride concentration of approximately 6 mg/L within 15 min. Consequently, the utilization of activated carbon derived from cow bones presents a viable approach for fluoride removal in natural water sources.

Keywords: Activated carbon; Adsorption; Cow bone; Defluoridation, Fluoride

1. Introduction

Fluoride (F^-) is a naturally occurring compound found in soil, water, and common mineral deposits. Fluoride-containing minerals are soluble, which dramatically increases the amount of fluoride in groundwater. The human body obtains fluoride primarily through water intake. Fluoride is an ingredient that helps strengthen bones and teeth (Whelton *et al.,* 2019). If the body receives an adequate dosage of fluoride, it has the potential to mitigate the incidence of dental caries among children and the prevalence of osteoporosis in the elderly. However, long-term consumption of water with elevated fluoride levels can lead to the development of dental fluorosis and skeletal abnormalities (Wei *et al.,* 2016; Guissouma *et al.,* 2017; Whelton *et al.,* 2019). Skeletal fluorosis, which can cause catastrophic damage to bones and joints, can occur when people use groundwater that contains fluoride higher than 4 mg/L (Kabir *et al.,* 2019). Additional health effects occurred from an excess of fluoride, such as acute gastroenteritis, rigidity in the muscles, anorexia, restlessness, sweating, dyspnea, and cardiac irregularities (Sahu *et al.,* 2017). Due to concerns about fluoride toxicity, the World Health Organization (WHO) has established a maximum fluoride concentration in public water supplies of 1.50 mg/L. Thailand has established a regulatory threshold for fluoride concentration in groundwater suitable for

consumption, mandating that it should not exceed 0.70 mg/L.

Previous studies have found high levels of fluoride contamination in groundwater and drinking water in many countries around the world (Ayoob, *et al.,* 2008; Yadav *et al.,* 2019; Solanki *et al.,* 2022). The United Nations Children's Fund (UNICEP) reports that over 10 million people are affected by fluoride contamination in water. In 25 countries worldwide, dental fluorosis is at risk from fluoridated water consumption (Petrone *et al.,* 2013). Notably, Thailand, specifically the northern region encompassing Chiang Mai, Lamphun, and Lampang provinces, has identified fluoride contamination in its groundwater sources. The majority of rural areas located in northern Thailand rely on groundwater as the primary source of raw water for the production of tap water. Groundwater is commonly treated by aeration, sedimentation, filtration, and disinfection before being distributed to households through the water pipeline system. Previously conducted research revealed that residents of the Buakhang sub-district, San Kamphaeng district, Chiang Mai province, continue to utilize tap water contaminated with fluoride for their drinking and culinary purposes. The exposure to fluoride through the consumption of drinking water averaged approximately 0.18 ± 0.10 mg/kg of body weight per day, while exposure via cooking water amounted to approximately 5.55 ± 3.52 mg/capita/day (Sawangjang *et al.,* 2019).

Lampang is one of the northern provinces of Thailand and is rich in fluoride minerals. Based on the 2019 survey conducted by the Lampang Provincial Groundwater Resources Office, which examined the fluoride levels in artesian wells within Lampang province, it was ascertained that fluoride concentrations exceeded the established standards in districts including Hang Chat, Ko Kha, Jae Hom, Thoen, Sop Prap, and Wang Nuea districts. The groundwater exhibits fluoride concentrations reaching as high as 5.9 mg/L. In the investigation examining the impact of fluoride in Ban Luam Klang, located within the Mae San Sub-district of Hang Chat district, Lampang province, the research revealed that 62.8% of children between the ages of 10 and 14 exhibited dental fluorosis (Kurupaporn, 2008). The severity of dental fluorosis increases with higher fluoride concentrations. In instances of mild symptoms, affected teeth may exhibit discernible white streaks that contrast with the natural dentin color. Conversely, in cases of severe fluorosis, the dentin may manifest a pronounced dark brown hue. When chewing or biting solids, the dentin is susceptible to fracturing, potentially leading to the development of bone abnormalities. Moreover, chronic exposure to water with fluoride concentrations of approximately 3 mg/L can lead to skeletal fluorosis and a higher likelihood of experiencing fractures (Peckham *et al.,* 2014; Helte *et al.,* 2021). Previous research has studied water fluoridation by reverse osmosis and nanofiltration (Shen and Schäfer, 2014), ion exchange (Yu *et al.,* 2021), and adsorption (He *et al.,* 2020). While techniques such as reverse osmosis, membrane separation, and ion exchange have demonstrated the capacity to diminish fluoride concentrations in water, there are limitations on the cost of membrane and ion exchange resin, the cost of operation, and the complexity of system operation. The process of adsorption exhibits suitability and feasibility when implemented in rural areas, given its efficacy in diminishing fluoride levels within water sources. Furthermore, the operation of this system does not entail significant complexity, and the adsorbents can be synthesized from readily available natural materials or waste products (Alkurdi *et al.,* 2019; He *et al.,* 2020; Pillai *et al.,* 2020). Therefore, the objectives of this research was to synthesize adsorbent material derived from cow bones and assess their effectiveness in adsorbing fluoride in both synthetic water samples and naturally occurring groundwater samples. Furthermore, the equilibrium and kinetics of fluoride adsorption were also studied. The adsorbent materials derived from cow bone in this study demonstrate their efficacy in removing fluoride concentrations in both synthetic and naturally occurring groundwater samples. The introduction of an economically viable and efficient approach to synthesizing adsorbent materials sourced from cow bones, is supported by experimental evidence, highlighting their application for defluoridation, particularly in Thailand.

2. Methodology

2.1 Activated cow bone preparation

Cow leg bones (CLB) were obtained from a local butcher shop located in Hang Chat district, Lampang province, Thailand. The CLB were washed and boiled in tap water to remove fat, bone marrow, and meat residues. Subsequently, the CLB were dried for 24 hours (h) and crushed to a size of 1-2 cm. They were soaked with acetone (Carlo Erba, France) for 30 minutes (min) to remove fat and protein residue and then washed with deionized (DI) water (Sutthi *et al.,* 2019). Afterward, they were dried in a hot air oven at 100 ºC for 24 h. These cow bone samples were used for the preparation of activated cow bones (ACB) using a pyrolysis process at 400, 500, and 600 ºC for 1, 2, and 3 h. The pyrolysis process employed a temperature ramp-up rate of 5 °C/min. ACB samples were washed with DI water repeatedly until a stable pH and low electrical conductivity (EC) were achieved in the washing solution, indicating the removal of all mineralized ash (Alkurdi *et al.,* 2020). Finally, they were dried for 24 h at 60 °C before being crushed. The crushed ACB were sieved using numbers 8 - 30 mesh (2.4 - 0.6 mm) and 30 - 50 mesh (0.6 - 0.3 mm), and stored in a desiccator for further studies.

2.2 Activated cow bone characterization

The ACB were characterized by morphology by field emission scanning electron microscopy, or FESEM (Apero S, ThermoFisher), surface area and pore size distribution by a Brunauer-Emmett-Teller or BET (Tristar II3020, Micromeritics) analyzer, point of zero charge analysis with a pH meter (SP-2100, Suntex), and functional group analysis by fourier transform infrared spectroscopy, or FT-IR (Invenio-S, Bruker). Furthermore, the volatile matter of the ACB was analyzed according to the standard method ASTM D5832-98 (Langama *et al.,* 2023), as illustrated in Table 1. Elevated levels of volatile matter in the ACB indicate an abundance of organic compounds, which is undesirable. The high volatile matter content tends to fill the pores of the ACB, resulting in a reduction of surface area and, consequently, adversely affecting the adsorption properties of the ACB (Lua & Yang, 2005).

2.3 Adsorption experiments

All experiments were conducted in batch mode. A synthetic water containing fluoride at 6 - 18 mg/L was prepared by dissolving sodium fluoride (NaF, Carlo Erba, France) in DI water. The experimental conditions were specified as follows: a 50 mL synthetic water sample; initial pH of water samples at 5, 7 and 9; shaken at 200 rpm at 30 ± 0.1 °C using a stackable shaker (MAXQ6000, Thermo Scientific); and reaction time of 5 - 180 min. The water sample was adjusted to the desired pH using 1 N hydrochloric acid (HCl, RCI Labscan, Thailand) and 1 N sodium hydroxide (NaOH, Carlo Erba, France), monitored by a pH meter (SP-2100, Suntex). The amounts of adsorbent were 0.25, 0.5, and 1 g. Before analysis, the water sample were filtered through a 0.45 μm pore-size nylon membrane filter (Filtrex, India). The filtered supernatant was then determined using a UV-Vis spectrophotometer (Genesys 10S UV-Vis, Thermo Scientific)

Table 1. Volatile matter content of ACB.

Pyrolysis temperature (°C)	Pyrolysis time (h)	Volatile matter (%)
400	1	15.43
400	2	15.59
400	3	15.46
500	1	12.55
500	2	8.39
500	3	8.40
600	1	5.52
600	2	6.27
600	3	9.40

at 570 nm with a reference solution as a blank according to the standard analytical method (APHA Method 4500-F-D). All experiments were conducted in duplicate. The average and standard deviation were determined. The statistical analysis of ACB pyrolysis temperatures and durations, ACB dosage, solution pH and initial fluoride concentration was conducted using one-way analysis of variance (ANOVA) with a significance level set at ≤ 0.05. The analysis was performed using the SPSS program version 18 (SPSS Inc., Chicago, IL).

The percentage of fluoride removal was calculated following Eq.1, and the adsorption capacity at equilibrium (q_e) was determined using Eq.2 (Dewage *et al.,* 2018).

$$\text{Fluoride removal (\%)} = \frac{C_i - C_f}{C_i} \times 100 \quad \text{(Eq.1)}$$

where C_i and C_f represent the initial and final concentration of fluoride in aqueous solution (mg/L).

$$q_e = \frac{V(C_0 - C_e)}{M} \quad \text{(Eq.2)}$$

where q_e is the amount of fluoride taken up by the adsorbent per unit mass of the ACB (mg/g), C_0 is the initial concentration of fluoride in the solution (mg/L), C_e is the final fluoride concentration in the solution (mg/L), V is the volume of the solution (L), and M is the weight of the ACB (g).

The efficacy of ACB in removing fluoride from naturally contaminated groundwater in the Hang Chat district, Lampang province, was investigated under optimal experimental conditions. The percentage of fluoride removal was determined using Eq.1. Two groundwater samples were collected in May 2022 from a village waterworks that relies on groundwater sources. The selection of this particular village for water sampling was based on the observation of the highest fluoride concentrations in its groundwater, approximately 6.36 ± 0.13 mg/L (Table 2).

Preliminary analyses of the physical and chemical properties of groundwater samples were conducted, encompassing color, turbidity, pH, iron, manganese, sulfate, chloride, fluoride, nitrate, total hardness, non-carbonate hardness, and total dissolved solids. All parameters were determined by the standard methods for the examination of water and wastewater (23rd edition). The physical and chemical properties of the groundwater are presented in Table 2. The results indicated that the groundwater generally exhibited good physical and chemical qualities. Nevertheless, the fluoride concentrations exceeded the standards, attributed to prevailing geographical conditions

Table 2. Physical and chemical properties of groundwater samples

Properties	Unit	Samples (Mean ± SD)	Standard value*
Color	Pt-Co	3.60 ± 0.00	5
Turbidity	NTU	0.26 ± 0.00	5
pH	mg/L	7.39 ± 0.00	7.00 - 8.50
Iron	mg/L	0.02 ± 0.01	≤ 0.5
Manganese	mg/L	0.25 ± 0.00	≤ 0.3
Sulfate	mg/L	0.02 ± 0.00	≤ 200
Chloride	mg/L	1.56 ± 0.01	≤ 250
Fluoride	mg/L	6.36 ± 0.13	≤ 0.7
Nitrate	mg/L	0.54 ± 0.02	≤ 45
Total hardness	mg/L as $CaCO_3$	29.00 ± 2.83	≤ 300
Non-carbonate hardness	mg/L as $CaCO_3$	24.39 ± 2.55	≤ 200
Total dissolved solids	mg/L	219.00 ± 1.41	≤ 600

Note: *The announcement by the Ministry of Natural Resources and Environment regarding the establishment of academic criteria and measures for public health prevention and environmental toxicity prevention, B.E. 2008.

2.4 Adsorption isotherm studies

An adsorption isotherm was employed to elucidate the interaction of the adsorbate. This step was crucial for optimizing the utilization of adsorbents and establishing an appropriate correlation for the equilibrium curve (Pragathiswaran *et al.,* 2013). There were numerous isotherm models that could be used to examine the mechanism of interaction between fluoride and adsorbents at equilibrium, including the Langmuir and Freundlich mathematical computations. Using common straight-line equations, the two fluoride parameters C_e and qe were connected to the plots of the Langmuir (Eq.3) and Freundlich (Eq.4) isotherms as follows:

$$\frac{1}{q_e} = \frac{1}{q_m} + \frac{1}{K_L q_m}\frac{1}{C_e} \qquad \text{(Eq.3)}$$

where C_e is the concentration of fluoride at equilibrium (mg/L) and q_e is the amount of fluoride adsorbed at equilibrium (mg/g). The Langmuir isotherm parameters include q_m (mg/g), b (L/mg) and K_L (L/mg) (Pasukphun & Suma, 2017).

$$\log q_e = [\log K_f + \left(\frac{1}{n}\right)\log C_e] \quad \text{(Eq.4)}$$

where C_e is the concentration at equilibrium (mg/L), q_e is the amount of fluoride adsorbed at equilibrium (mg/g), K_f are Freundlich isotherm parameters, and n is the heterogeneity factor. K_f and n can be examined from a linear plot of log q_e against log C_e (Yasim *et al.,* 2016).

2.5 Adsorption kinetic studies

The pseudo-first-order and pseudo-second-order were frequently employed in kinetic studies to verify the fit of the experimental data for ACB to identify the adsorption rate and mechanism of fluoride onto ACB. The pseudo-first-order and pseudo-second-order equations can be computed using Eq.5 and 6, respectively. (Akbar *et al.,* 2016).

$$\log (q_e - q_t) = \log q_e - \frac{tk_1}{2.303} \qquad \text{(Eq.5)}$$

$$\frac{t}{q_t} = \frac{1}{k_2 q_e^2} + \frac{t}{q_e} \qquad \text{(Eq.6)}$$

where the quantities of fluoride adsorbed (mg/g) at equilibrium are represented by q_e and q_t at any given time t (min). The slope of the log (q_e-q_t) vs. t graph can be used to determine the value of the adsorption rate constant, or k_1. k_2 is the adsorption rate constant in the pseudo-second order. Since the adsorption rate constant, k_2, can be calculated from the intercept of the curve, linear regression was achieved for this model from the plot of t/q_t vs. t.

3. Results and Discussion

3.1 Characteristic of activated cow bone

3.1.1 Morphology

The texture and dimensions of raw cow bone and ACB calcined at temperatures ranging from 400 - 600 °C for 1-3 h were imaged with FESEM at a magnification of 5,000x, as shown in Figures 1 (a)-(j). The comparative analysis revealed distinct textural and particle morphology differences between raw cow bone and ACB. The ACB exhibited a well-defined, interconnected, porous structure. The formation of hydroxyapatite crystals on cow bones occurred due to changes in the chemical composition of the bones, facilitated by the removal of organic constituents achieved through high-temperature processing (Shahid *et al.,* 2020).

3.1.2 Surface area and pore size distribution

Table 3 presents the surface area measurements for raw cow bone and ACB at various pyrolysis temperatures and durations. Notably, ACB subjected to a 1-h pyrolysis at 600 °C exhibited the most substantial surface area, measuring approximately 144.20 m²/g. A prior investigation revealed that cow bone char exhibited the greatest surface area at 103.11 m²/g, surpassing pig bone char at 83.79 m²/g, and chicken bone char at 62.80 m²/g (Sawangjang *et al.,* 2021). Elevating the pyrolysis temperature leads to an expansion in surface area, primarily attributable to the devolatilization process that removes select biological components from the biomass (Brunson & Sabatini, 2014).

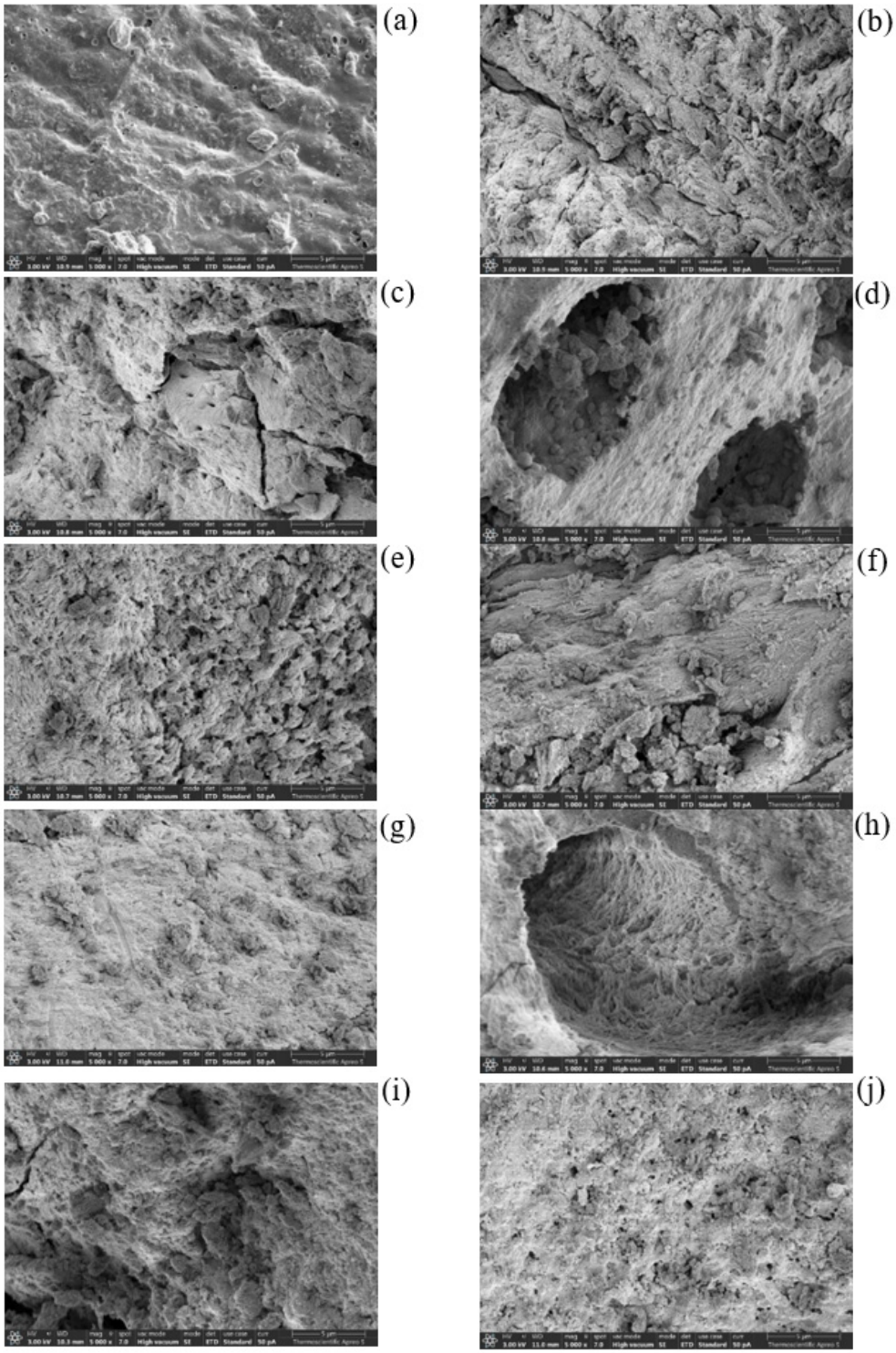

Figure 1. FESEM morphology of (a) raw cow bone; (b) ACB 400 °C, 1 h; (c) ACB 400 °C, 2 h; (d) ACB 400 °C, 3 h; (e) ACB 500 °C, 1 h; (f) ACB 500 °C, 2 h; (g) ACB 500 °C, 3 h; (h) ACB 600 °C, 1 h; (i) ACB 600 °C, 2 h; (j) ACB 600 °C, 3 h at 5,000x magnification.

3.1.3 Points of zero charge

Results of the ACB's point of zero charge (PZC) investigation are displayed in Figure 2. The results indicated that ACB exhibited a PZC of approximately 7.4, aligning closely with the previously reported PZC value of 7.90 for cow bone char (Sawangjang *et al.,* 2021). Generally, protonation occurs when the adsorbent surface becomes positively charged, typically when the pH of the solution falls below the PZC. Conversely, deprotonation takes places as the adsorbent material surface acquires a negative charge, which happens when the pH of the solution surpasses the PZC (Medellin-Castillo *et al.,* 2014). The pKa of fluoride is 3.17; when the solution's pH surpasses this threshold, fluoride ions become negatively charged. Consequently, fluoride ions exhibit a pronounced affinity for adsorption onto the ACB surface within the pH range defined by the pKa (3.17) and the PZC (7.4) of the ACB.

3.1.4 FT-IR analysis

Figure 3 exhibits the FT-IR spectrum of raw cow bone and the ACB at 400, 500, and 600 °C. The results found that six functional groups were identified by the study of raw cow bones. The hydroxyl (O - H) functional group's peak is estimated to be 3302 1/cm. The C - H functional group is represented by peaks at roughly 2920 and 2850 1/cm. The carbonyl functional group (C = O) peaks at approximately 1449; 1410 and 873 1/cm indicate the carbonate functional group (CO_3^{2-}), which peaks at approximately 1018 1/cm; and the C-H function, which peaks at approximately 1741 1/cm. The phosphate functional group (PO_4^{3-}) is shown by the peaks at 961 and 602 1/cm, while the calcium (Ca) function is represented by the peak at around 560 1/cm (Rojas-Mayorga *et al.,* 2015; Akindoyo *et al.,* 2019). The C – H functional groups were found in raw cow bone due to the presence of various organic constituents. In contrast, the ACB showed no C – H functional group, indicating the complete removal of various organic substances in cow bones after incineration and resulting in a pure hydroxyapatite structure (Akindoyo *et al.,* 2019). The hydroxyapatite structure of the ACB remained unchanged even with increased temperature and duration of pyrolysis.

3.2 Effect of pyrolysis temperatures and durations

The result of fluoride removal conducted at an initial concentration of approximately 6 mg/L and pH 5 using 0.5 g of ACB subjected to various pyrolysis temperatures (400, 500, and 600 °C) and durations (1, 2, and 3 h), utilizing mesh sizes ranging from 30 to 50, is illustrated in Figure 4 (a – c). The findings indicate rapid fluoride adsorption during the initial phase (time < 15 min), followed by a subsequent period of slower adsorption rate. In the initial 15 min, larger amounts of fluoride were removed due to the rapid binding of fluoride ions to the readily accessible active sites on the outer surface of the ACB. ACB subjected to pyrolysis temperatures of 500 and 600 °C exhibited a significantly enhanced fluoride absorption rate compared to ACB calcined at 400 °C, in line with the surface

Table 3. Surface area of raw cow bone and ACB.

Adsorbents	Pyrolysis temperature (°C)	Pyrolysis time (h)	Surface area (m^2/g)
Raw cow bone	-	-	1.19
ACB	400	1	108.76
ACB	400	2	118.13
ACB	400	3	133.24
ACB	500	1	134.28
ACB	500	2	125.61
ACB	500	3	138.28
ACB	600	1	144.20
ACB	600	2	138.59
ACB	600	3	135.85

area data presented in Table 3. This result indicates that the calcination temperature of ACB influenced both the surface area and the efficiency of fluoride absorption. Specifically, ACB calcined at 600 °C for 1 h, which exhibited the highest surface area, demonstrated the most effective fluoride absorption capability (83.91 ± 6.25% in 180 min), as depicted in Figure 4. Raising the pyrolysis temperature was observed to have a direct correlation with an increase in both the surface area and pore volume of the charred material. This phenomenon is attributed to the devolatilization process affecting specific constituents within the biomass (Brunson & Sabatini, 2014). When comparing the ACB subjected to pyrolysis temperatures of 400, 500, and 600 °C, the results indicated that the removal percentages of fluoride were not significantly different ($p > 0.05$, with p-values of 0.65, 0.96, and 0.90 for durations of 1, 2, and 3 h, respectively).

At higher temperatures, particularly 600 °C, more of the organic components in the bone are effectively decomposed and burnt off. This includes collagen, proteins, and any other organic materials present in the bone. These organic materials can take up a significant amount of space within the bone's structure. When they are removed during calcination, it leaves behind pores and voids, resulting in a greater surface area.

The higher surface area observed in activated cow bone calcined at 600 °C for 1 h compared to samples calcined for 2 and 3 h can be attributed to the intricate dynamics of the calcination process influencing the bone structure. The initial 1-h calcination period facilitates the efficient removal of organic matter and water, initiating the formation of a porous structure within the bone matrix, ultimately contributing to an augmented surface area. This observed phenomenon suggests an optimal balance achieved during the 1-h calcination, allowing for porosity development without succumbing to over-burning or excessive sintering. Prolonged calcination times (2 or 3 h) lead to potential over-burning or sintering, causing a reduction in surface area due to the collapse of pores. Additionally, extended exposure to high temperatures induces structural changes compromising the bone's ability to maintain a high surface area.

3.3 Effect of ACB dosage and particle size

Figures 5 and 6 illustrate the effects of ACB dosage and particle size, respectively. ACB calcined at 600 °C for 1 h, chosen for its highest efficiency, was employed to investigate these effects. The experiments were conducted with a fixed fluoride concentration of approximately 6 mg/L and a solution pH of 5. The results showed that 0.25, 0.5, and 1 g of ACB could absorb fluoride up to 77.77 ± 4.95, 83.91 ± 6.25, and 71.35 ± 10.54 %, respectively, at a 180 - min adsorption times (Figure 5). The removal percentages of fluoride at varying ACB dosages were not statistically

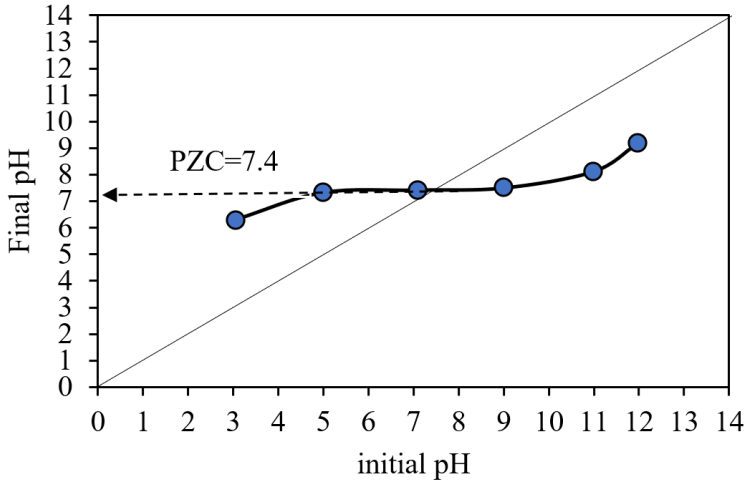

Figure 2. ACB's point of zero charge (PZC).

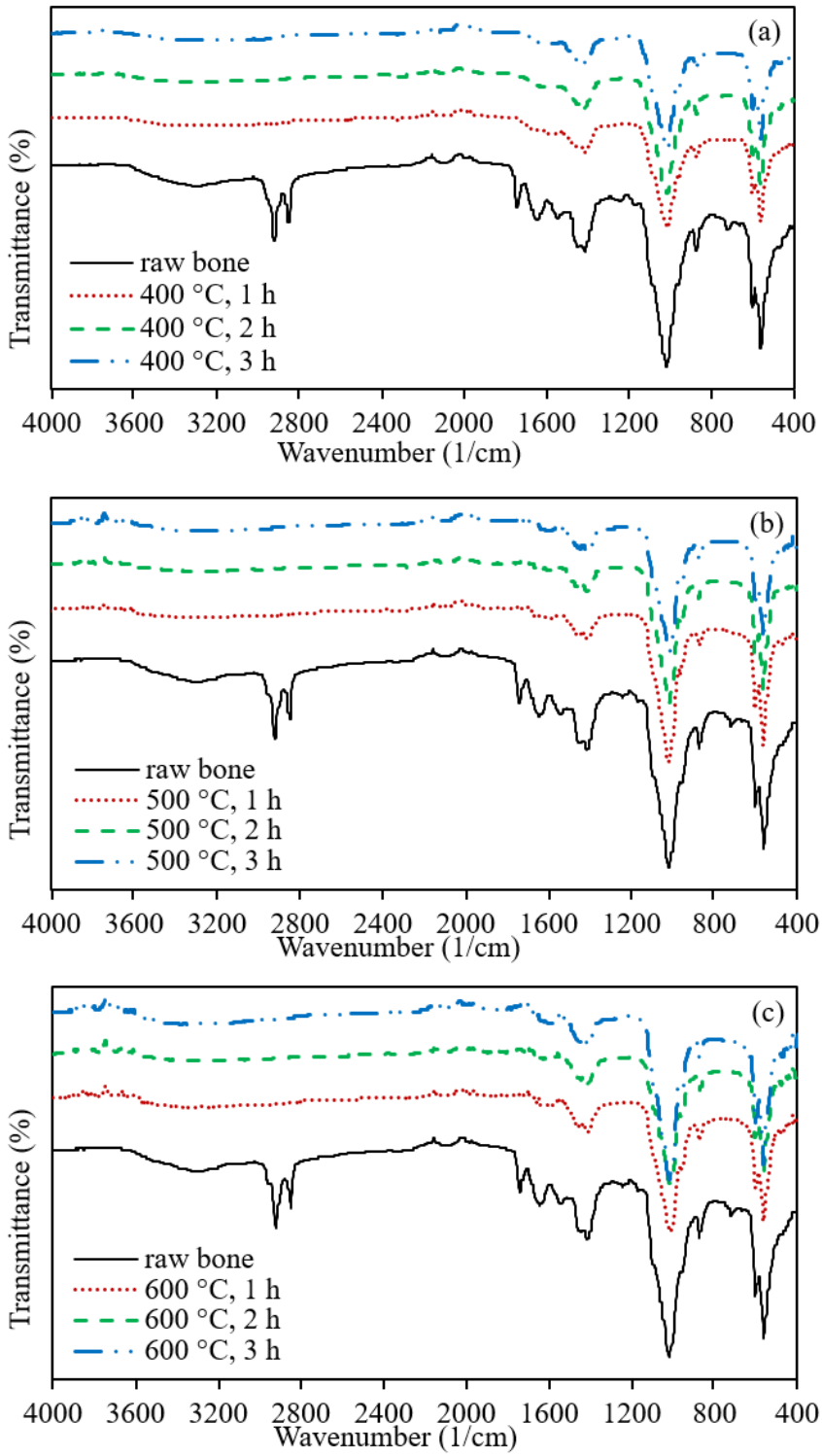

Figure 3. FT-IR spectrum of raw cow bone and ACB subjected to pyrolysis temperatures of (a) 400 °C, (b) 500 °C, and (c) 600 °C for durations ranging from 1-3 h.

significant ($p > 0.05$, with a p-value of 0.85). Notably, the efficiency in fluoride removal was higher when using 0.5 g of ACB compared to both 0.25 g and 1 g. The utilization of a lesser quantity of ACB (0.25 g) proved inadequate, either impeding the adsorption process or resulting in an insufficient ACB supply for absorption. Conversely, excessive application of ACB (1 g) may lead to undesirable particle aggregation or overlapping, diminishing the overall surface area available for adsorption. In the case of ACB sizes, specifically 8 - 30 mesh (2.4 - 0.6 mm) and 30-50 mesh (0.6 - 0.3 mm), the most effective fluoride absorption rates were achieved at 73.72 ± 1.92 and 83.91 ± 6.25%, respectively, as illustrated in Figure 6.

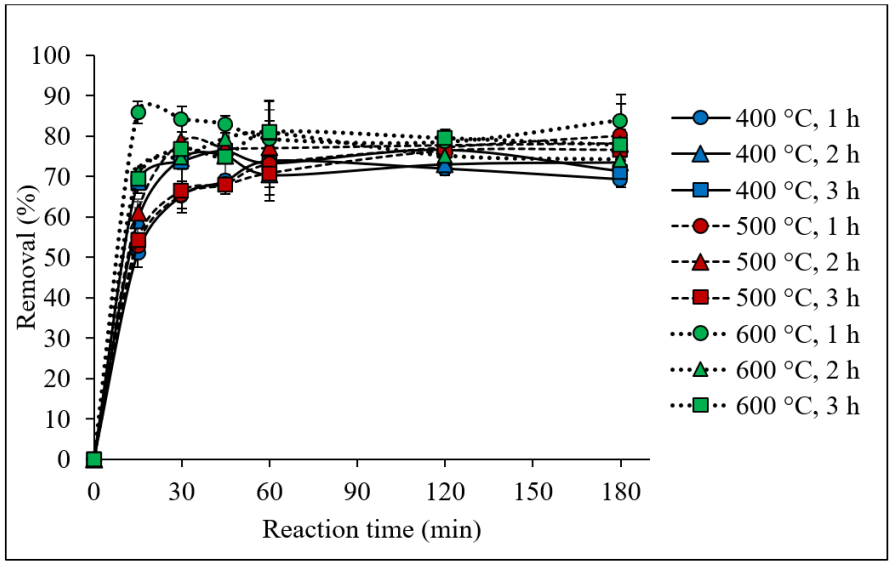

Figure 4. Fluoride removal efficiency of ACB subjected to pyrolysis temperatures of 400, 500, and 600 °C for durations ranging from 1-3 h.

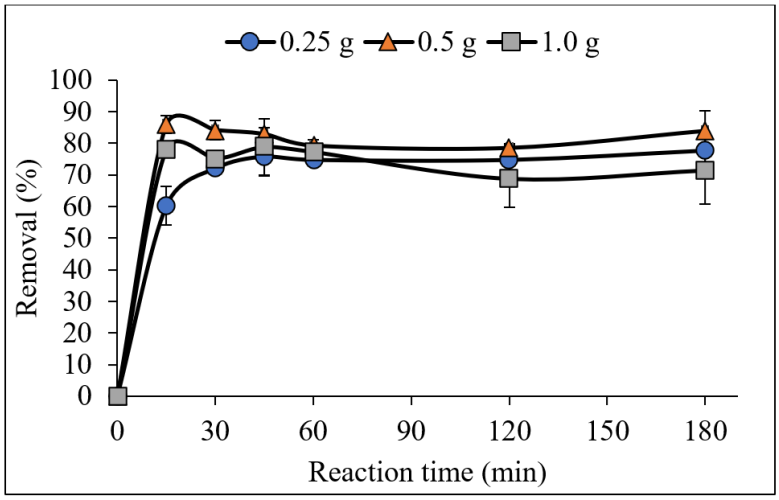

Figure 5. Fluoride removal efficiency using 0.25, 0.5, and 1 g of 30 - 50 mesh ACB subjected to pyrolysis temperatures of 600 °C for 1 h.

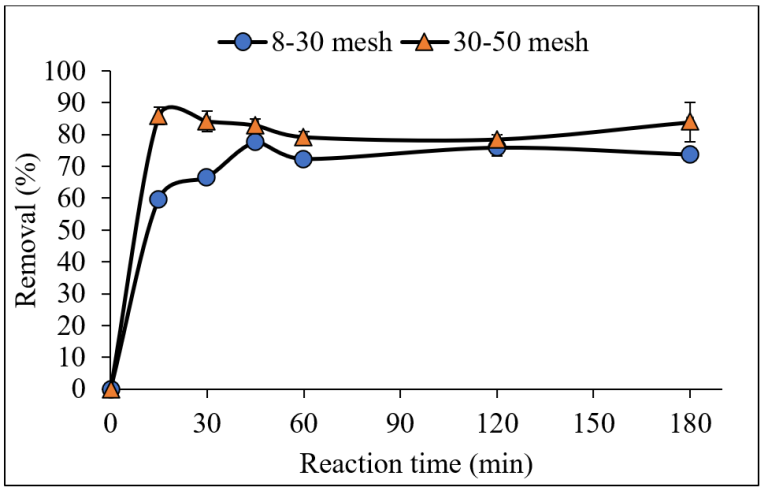

Figure 6. Fluoride removal efficiency using 8 - 30 mesh and 30-50 mesh of 0.5 g ACB subjected to pyrolysis temperatures of 600 °C for 1 h.

3.4 Effect of solution pH

Figure 7 presents the effect of varying solution pH levels, ranging from 5 to 9, on the efficiency of fluoride removal. This experiment was conducted with approximately 6 mg/L of fluoride concentration and 0.5 g of 30 - 50 mesh ACB subjected to pyrolysis temperatures of 600 °C for 1 h. The findings indicate that, after 180 min adsorption time, initial pH values of 5, 7, and 9 resulted in fluoride absorption rates of 83.91 ± 6.25, 76.63 ± 0.00, and 75.80 ± 1.37%, respectively. The removal percentages of fluoride at different solution pH levels were not significantly different ($p > 0.05$, with a p-value of 0.90). The pH value of 5 exhibited the highest and most rapid fluoride removal. The diminishing efficiency of fluoride removal with increasing pH levels can likely be attributed to a competitive interaction between hydroxyl groups and fluoride ions within the alkaline environment, as noted by Fung *et al.* (2021). At pH levels below the PZC (7.4), the surface charge of the ACB becomes positively charged, thereby enhancing the attraction of negatively charged fluoride ions for adsorption onto the ACB, as described in Section 3.1.3.

3.5 Effect of initial fluoride concentration

The results regarding the effect of initial fluoride concentration on fluoride removal efficiency are depicted in Figure 8. For this experiment, the conditions were set at pH 5 with 0.5 g of 30 - 50 mesh ACB subjected to pyrolysis temperatures of 600 °C for 1 h. After 180 min of adsorption time, fluoride removal rates reached 83.91 ± 6.25, 77.79 ± 0.34, and 72.78 ± 1.71 % for initial fluoride concentrations of approximately 6, 12, and 18 mg/L, respectively. The removal percentages of fluoride at different initial fluoride concentration were not significantly different ($p > 0.05$, with a p-value of 0.73). Notably, the aqueous solution with the lowest initial fluoride concentration exhibited the highest degree of fluoride removal, a trend that can be rationalized by considering the availability of adsorption sites. At lower initial fluoride concentrations, more adsorption sites are accessible. Conversely, at higher initial fluoride concentrations, the solution becomes enriched with fluoride ions, saturating adsorption sites and leaving a significant portion of fluoride ions unabsorbed (Tan *et al.,* 2020). During the initial 15 min, the adsorption process exhibited a notably rapid rate, emphasizing its association with external surface adsorption, irrespective of the concentration. Subsequently, as equilibrium was approached, the rate gradually declined, indicating a transition towards internal surface adsorption (Djilani *et al.,* 2016).

3.6 Adsorption capacity

The maximum adsorption capacity of ACB is detailed in Table 4. It was observed that ACB calcined at 600°C for 1 h had a maximum capacity of 0.52 mg/g. This suggests that the fluoride adsorption capacity is influenced by the surface area, as supported by the fact that ACB calcined at 600 °C for 1 h exhibited the highest surface area, as presented in Table 3. A previous study also confirmed that the capacity for fluoride adsorption was predominantly influenced by the surface area of the bone char rather than the hydroxyapatite content (Sawangjang *et al.,* 2021).

3.7 Adsorption isotherm studies

Figure 9 depicts the application of the Langmuir and Freundlich models to identify the adsorption isotherms. The isotherms were calculated using the data collected for fluoride concentrations ranging from 6 to 18 mg/L. The slopes, intercepts, and associated correlation coefficients of these data were used to calculate the adsorption constants for both models, as presented in Table 5. The findings of this study align with previous research indicating consistent fluoride adsorption behavior with the Langmuir model (Tan *et al.,* 2020; Yang *et al.,* 2022). The Langmuir adsorption isotherm assumes a certain

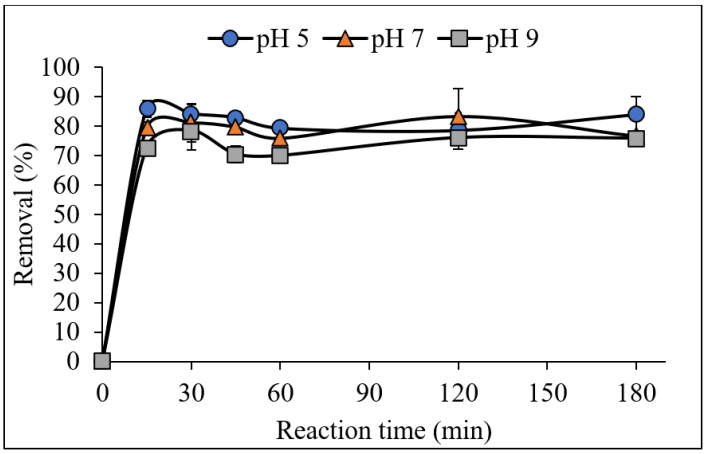

Figure 7. Effect of initial pH on the adsorption of fluoride by 0.5 g of 30 - 50 mesh ACB subjected to pyrolysis temperatures of 600 °C for 1 h.

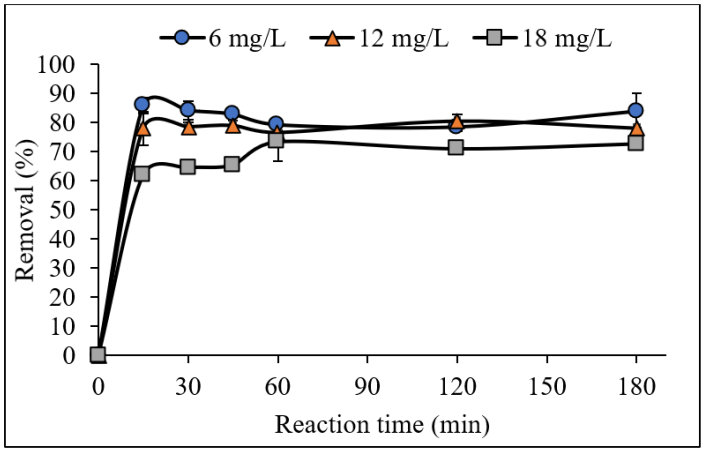

Figure 8. Effect of initial fluoride concentration on the adsorption of fluoride by 0.5 g of 30 - 50 mesh ACB subjected to pyrolysis temperatures of 600 °C for 1 h.

number of adsorbed molecules with specific adsorption positions, representing single-layer adsorption. It implies that only one molecule of the sorbate is adsorbed for each molecule of the sorbent material. The heat of adsorption is equal and constant at each position, with no forces acting between molecules in close proximity, and the adsorption energy is uniform across the adsorbent material (Sawangjang *et al.,* 2021; Leyva-Ramos *et al.,* 2010). The Langmuir adsorption constant and the initial concentration of fluoride on the adsorbent are used to calculate the separation factor (RL), expressed as Eq.7 (Moussavi & Khosravi, 2011).

$$R_L = \frac{1}{1+K_L C_0} \quad \text{(Eq.7)}$$

The interpretation of the separation factor can be categorized into four scenarios: $R_L > 1$ indicates inconsistency with the adsorption isotherm (unfavorable), $R_L = 1$ denotes a linear adsorption isotherm, $0 < R_L < 1$ signifies a favorable adsorption isotherm (favorable), and $R_L = 0$ signifies an irreversible adsorption isotherm (irreversible). From Table 5, it was determined that the R_L fell within the range of 0.02 - 0.58, indicating effective adsorption behavior consistent with the Langmuir adsorption isotherm.

Table 4. Maximum adsorption capacity of ACB

Adsorbents	Pyrolysis temperature (°C)	Pyrolysis durations (h)	Maximum adsorption capacity (mg/g)
ACB	400	1	0.43
ACB	400	2	0.15
ACB	400	3	0.09
ACB	500	1	0.50
ACB	500	2	0.17
ACB	500	3	0.10
ACB	600	1	0.52
ACB	600	2	0.16
ACB	600	3	0.09

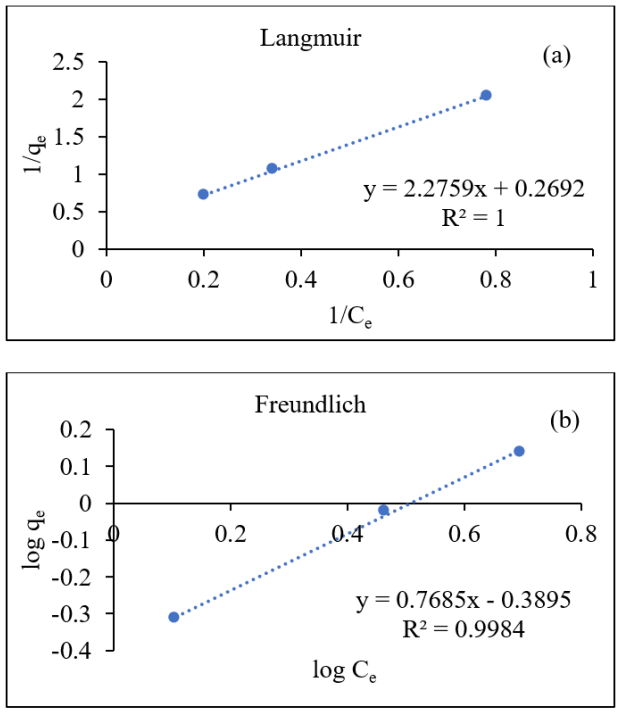

Figure 9. Adsorption isotherm curves of fluoride onto ACB; (a) Langmuir isotherm and (b) Freundlich isotherm

Table 5. Langmuir and Freundlich model constants and correlation coefficients of ACB with calcined at 600 °C, 1 h for fluoride adsorption

Langmuir isotherm				Freundlich isotherm		
q_m (mg/g)	K_L (L/mg)	R_L	R^2	K_F (mg/g)(L/mg)$^{1/n}$	1/n	R^2
3.757	0.116	0.02-0.58	1.000	0.406	0.771	0.9984

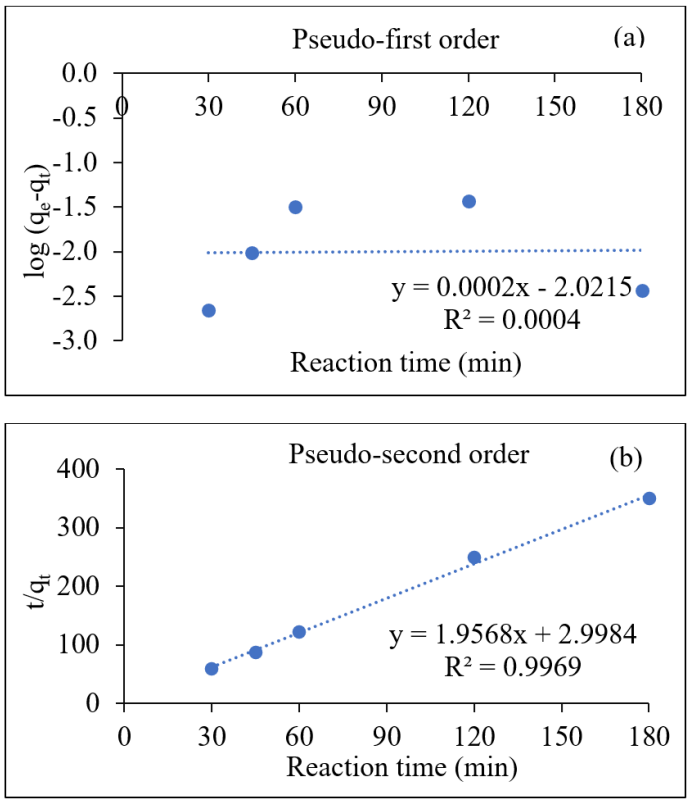

Figure 10. Adsorption kinetic curves of fluoride onto ACB calcined at 600 °C for 1 h: (a) pseudo-first-order model, (b) pseudo-second-order model

3.8 Adsorption kinetic studies

The kinetics and mechanism of fluoride adsorption in ACB calcined at 600 °C for 1 h were investigated using pseudo-first-order and pseudo-second-order models. The pseudo-first-order model signifies an adsorption reaction preceded by diffusion through a boundary, while the pseudo-second-order model is typically associated with an adsorption process in which chemisorption governs the rate (He *et al.,* 2016). Figure 10 and Table 6 display the fitting plots and corresponding parameters of the pseudo-first-order and pseudo-second-order models, respectively. The results indicate that the pseudo-second-order model provides a more suitable fit for fluoride adsorption, demonstrated by its higher correlation coefficient ($R^2 = 0.9969$) compared to the pseudo-first-order model ($R^2 = 0.0004$). This suggests that the primary rate-determining process is likely chemisorption, which involves the formation of covalent bonds through the sharing or exchange of electrons between the anion and the adsorbent (Tan *et al.,* 2020).

Table 6. Kinetic model parameters of fluoride adsorption onto ACB calcined at 600 °C for 1 h

q_e experiment (mg/g)	Pseudo-first order			Pseudo-second order		
	q_e calculated (mg/g)	k_1 (1/min)	R^2	q_e calculated (mg/g)	k_2 (1/min)	R^2
0.52	105.08	0.0005	0.0004	0.51	1.277	0.9969

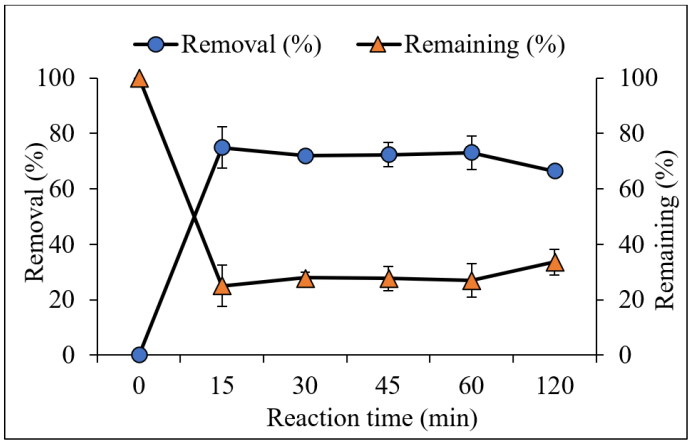

Figure 11. ACB on fluoride adsorption efficiency and the remaining fluoride percentage in natural groundwater samples

The experimentally determined equilibrium adsorption capacity (q_e) in this study was 0.52 mg/g, slightly surpassing the reported q_e value for cow bone char in the preceding study (0.50 mg/g). Furthermore, the q_e values determined through pseudo-first-order and pseudo-second-order calculations in this study exceeded those reported in the preceding study, which were 1.00 and 0.50 mg/g, respectively (Sawangjang *et al.,* 2021).

3.9 Application of ACB on fluoride adsorption efficiency in natural groundwater samples

Figure 11 displays the efficiency of ACB in removing fluoride and the remaining fluoride percentage in natural groundwater samples. Adsorption experiments were conducted using 0.5 g of ACB calcined at 600 °C for 1 h, with a size of 30 - 50 mesh and a solution pH of 5. The results reveal that fluoride adsorption was effective, reaching up to 74.95 ± 7.38 % in 15 min. It is evident that the efficacy of ACB in adsorbing fluoride in natural groundwater sample was lower compared to that in synthetic water. This discrepancy can be attributed to the presence of additional minerals in groundwater, which may compete for absorption with fluoride. Previous studies have reported that sulfate, chloride, and nitrate can compete with fluoride ions for the active sorption sites present in the sorbent, consequently diminishing the sorbent's ability to remove fluoride ions (Nigri *et al.,* 2017).

4. Conclusion

The key findings of the study highlight the superior fluoride adsorption capabilities of ACB subjected to a 1-h calcination process at 600 °C. This superiority is particularly evident in synthetic water samples with around 6 mg/L of fluoride, compared to ACB calcined at 400 and 500 °C. This heightened performance is attributed to its significantly larger surface area (144.20 m^2/g), enabling a remarkable fluoride adsorption rate of approximately 85.87 ± 2.78 % within just 15 min, with an optimal ACB amount of 0.5 g and particle size of 30 - 50 mesh. Notably, variations in initial pH levels revealed that pH 5 enhances fluoride adsorption efficiency compared to pH 7 and 9. The escalation

of initial fluoride concentrations from 6 to 12 and 18 mg/L resulted in a decrease in adsorption efficiency. The effect of pyrolysis temperature and duration, ACB dosage, solution pH, and initial fluoride concentration were not significantly different ($p > 0.05$). The maximum adsorption capacity of ACB was determined to be 0.52 mg/g. Kinetic studies established that fluoride adsorption adheres to the Langmuir isotherm model and aligns well with the pseudo-second-order model, suggesting a chemisorption-dominated mechanism. Furthermore, the study demonstrated ACB's potential to adsorb fluoride from naturally occurring groundwater, achieving an adsorption rate of approximately 74.95 ± 7.38 % within 15 min at an initial fluoride concentration of approximately 6 mg/L. This signifies the feasibility of using ACB for fluoride removal in natural water sources. However, the study emphasizes the need for further investigations, particularly in areas such as cost-effectiveness and public acceptance.

Acknowledgement

This study received support from the Faculty of Public Health Research Fund, Thammasat University, Fiscal Year B.E.2563, Contract No.1/64, and the Faculty of Public Health Research Fund, Thammasat University, Fiscal Year B.E.2565 (Student Research and Academic Assistance Fund, No.182/2565). The authors express their gratitude to Mr. Kittiphong Youdee for his invaluable support in the laboratory and to all the staff members at the Faculty of Public Health, Thammasat University, for their assistance.

References

Akbar NA, Aziz HA, Adlan MN. Potential of high-quality limestone as adsorbent for iron and manganese removal in groundwater. Jurnal Teknologi 2016; 78(9-4): 77-82.

Akidndoyo JO, Ghazali S, Beg MDH, Jeyaratnam N. Characterization and elemental quantification of Natural hydroxyapatite produced from cow bone. Chemical Engineering Technology 2019;42(9): 1805-1815.

Alkurdi SSA, Al-Juboori RA, Bundschuh J, Hamawand I. Bone char as a green sorbent for removing health threatening fluoride from drinking water. Environment International 2019; 127: 704-719.

Alkurdi SSA, Al-Juboori RA, Bundschuh J, Bowtell L, McKnight S. Effect of pyrolysis conditions on bone char characterization and its ability for arsenic and fluoride removal. Environmental Pollution 2020; 262: 114221.

Ayoob S, Gupta A, Bhat VT. A conceptual overview on sustainable technologies for the defluoridation of drinking water. Critical Reviews in Environmental Science and Technology 2008; 38(6): 401-470.

Brunson LR, Sabatini DA Role of surface area and surface chemistry during an investigation of eucalyptus wood char for fluoride adsorption from drinking water. Journal of Environmental Engineering 2014; 141: 1-8.

Dewage NB, Liyanage AS, Pittman CU, Mohan D, Mlsna T. Fast nitrate and fluoride adsorption and magnetic separation from water on α-Fe_2O_3 and Fe_3O_4 dispersed on Douglas fir biochar. Bioresource Technology 2018; 263: 258-265.

Djilani C, Zaghdoudi R, Djazi F, Bouchekima B, Lallam A, Magri P. Preparation and characterisation of activated carbon from animal bones and its application for removal of organic micropollutants from aqueous solution. Desalination and Water Treatment 2016; 57(52): 25070-25079.

Fung E, Johnson KI, Li W, Borges W, Chi K, Sharma SK, Madan Y, Sharma PR, Hsiao BS. Study the use of activated carbon and bone char on the performance of gravity sand-bag water filter. Membranes (Basel) 2021; 11(11): 868.

Guissouma W, Hakami O, Al-Rajab AJ, Tarhouni J. Risk assessment of fluoride exposure in drinking water of Tunisia. Chemosphere 2017; 177: 102-108.

He J, Cai X, Chen K, Li Y, Zhang K, Jin Z, Meng F, Liu N, Wang X, Kong L, Huang A, Liu J. Performance of a novelty-defined zirconium metal-organic frameworks adsorption membrane in fluoride removal. Journal of Colloid and Interface Science 2016; 484: 162-172.

He J, Yang Y, Wu Z, Xie C, Zhang K, Kong L, Liu J. Review of fluoride removal from water environment by adsorption, Journal of Environmental Chemical Engineering 2020; 8(6): 104516.

Helte E, Donat Vargas C, Kippler M, Wolk A, Michaëlsson K, Åkesson A. Fluoride in drinking water, diet, and urine in relation to bone mineral density and fracture incidence in postmenopausal women. Environmental Health Perspectives 2021; 129(4): EHP7404.

Kabir H, Gupta AK, Tripathy S. Fluoride and human health: systematic appraisal of sources, exposures, metabolism, and toxicity. Critical Reviews in Environmental Science and Technology 2019; 50: 1-78.

Kuruphaporn Y. Drinking behavior in Banlumklang villagers, Mae San Subdistrict, Hang Chat District, Lampang Province, a high fluoride content in water area. Dental Public Health Science 2008; 13(3): 20-26.

Langama P, Anguile J, Bissielou C, Bouraïma A, Ndong A, Kouotou D, Mbadcam J. Preparation and characterization of activated carbons from asparagus palm (*Laccosperma robustum*) bark by chemical activation with H_3PO_4 and KOH. American Journal of Analytical Chemistry 2023; 14: 55-71.

Leyva-Ramos R, Rivera-Utrilla J, Medellin-Castillo N, Sanchez-Polo M. Kinetic modeling of fluoride adsorption from aqueous solution onto bone char. Chemical Engineering Journal 2010; 158: 458-467.

Lua A, Yang T. Characteristics of activated carbon prepared from pistachio-nut shell by zinc chloride activation under nitrogen and vacuum conditions. Journal of Colloid and Interface Science 2005; 290: 505-513.

Medellin-Castillo AN, Leyva-Ramos R, Padilla-Ortega E, Ocampo Perez R, Flores-Cano JV, Berber-Mendoza MS. Adsorption capacity of bone char for removing fluoride from water solution. Role of hydroxyapatite content, adsorption mechanism and competing anions. Journal of Industrial and Engineering Chemistry 2014; 20: 4014-4021.

Moussavi G, Khosravi R. The removal of cationic dyes from aqueous solutions by adsorption onto pistachio hull waste. Chemical Engineering Research and Design 2011; 89: 2182-2189.

Nigri EM, Cechinel MAP, Mayer DA, Mazur LP, Loureiro JM, Rocha SDF, Vilar VJP. Cow bones char as a green sorbent for fluorides removal from aqueous solutions: batch and fixed-bed studies. Environmental Science and Pollution Research 2017; 24: 2364-2380.

Pasukphun N, Suma S. Preliminary study of color removal from Moh Hom dyeing wastewater using a low cost activated carbon derived from pineapple waste. Applied Environmental Research 2017; 39(3): 41–47.

Peckham S, Awofeso N. Water fluoridation: a critical review of the physiological effects of ingested fluoride as a public health intervention. Scientific World Journal 2014; 2014:1-10.

Petrone P, Guarino FM, Giustino S, Gombos F. Ancient and recent evidence of endemic fluorosis in the Naples area. Journal of Geochemical Exploration 2013; 131: 14-27.

Pillai P, Dharaskar S, Shah M, Sultania R. Determination of fluoride removal using silica nano adsorbent modified by rice husk from water. Groundwater for Sustainable Development 2020; 11: 100423.

Pragathiswaran C, Sibi S, Sivanesan P. Comparison studies of various adsorption isotherms for aloevera adsorbent. International Journal of Research in Pharmacy and Chemistry 2013; 3(4): 886-889.

Rojas-Mayorga CK, Bonilla-Petriciolet A, Silvestre-Albero J, Aguayo-Villarreal IA, Mendoza-Castillo DI. Physico-chemical characterization of metal-doped bone chars and their adsorption behavior for water defluoridation. Applied Surface Science 2015; 355: 748-760.

Sahu BL, Banjare GR, Ramteke S, Patel KS, Matini L. Fluoride contamination of groundwater and toxicities in dongargaon block, Chhattisgarh, India. Exposure and Health 2017; 9: 143-156.

Sawangjang B, Hashimoto T, Wongrueng A, Wattanachira S, Takizawa S. Assessment of fluoride intake from groundwater and intake reduction from delivering bottled water in Chiang Mai Province, Thailand. Heliyon 2019; 5: e02391.

Sawangjang B, Induvesa P, Wongrueng A, Pumas C, Wattanachira S, Rakruam P, Punyapalakul P, Takizawa S, Khan E. Evaluation of fluoride adsorption mechanism and capacity of different types of bone char. International Journal of Environmental Research and Public Health 2021; 18: 6878.

Shahid MK, Kim JY, Shin G, Choi Y. Effect of pyrolysis conditions on characteristics and fluoride adsorptive performance of bone char derived from bone residue. Journal of Water Process Engineering 2020; 37: 101499.

Shen J, Schäfer A. Removal of fluoride and uranium by nanofiltration and reverse osmosis: A review. Chemosphere 2014; 117: 679-691.

Solanki YS, Agarwal M, Gupta AB, Gupta S, Shukla P. Fluoride occurrences, health problems, detection, and remediation methods for drinking water: A comprehensive review. Science of The Total Environment 2022; 807(1): 150601.

Sutthi N, Pranudta A, Padungthon S, Laonapakul T. Fluoride reduction in water using cow and fish bones. Farm Engineering and Automation Technology Journal 2019; 5(1): 49-57.

Tan TL, Krusnamurthy P, Nakajima H, Rashid SA. Adsorptive, kinetics and regeneration studies of fluoride removal from water using zirconium-based metal organic frameworks. RSC Advances 2020; 10: 18740-18752.

Wei C, Guo H, Zhang D, Wu Y, Han S, An Y, Zhang F. Occurrence and hydrogeochemical characteristics of high-fluoride groundwater in Xiji County, southern part of Ningxia Province, China. Environmental Geochemistry and Health 2016; 8(1): 275-290.

Whelton HP, Spencer AJ, Do LG, Rugg-Gunn AJ. Fluoride revolution and dental caries: evolution of policies for global use. Journal of Dental Research 2019; 98: 837-846.

Yadav KK, Kumar S, Pham QB, Gupta N, Rezania S, Kamyab H, Yadav S, Vymazal J, Kumar V, Tri DQ, Talaiekhozani A, Prasad S, Reece LM, Singh N, Maurya PK, Cho J. Fluoride contamination, health problems and remediation methods in Asian groundwater: A comprehensive review. Ecotoxicology and Environmental Safety 2019; 182: 109362.

Yang Y, Li X, Gu Y, Lin H, Jie B, Zhang Q, Zhang X Adsorption property of fluoride in water by metal organic framework: Optimization of the process by response surface methodology technique. Surfaces and Interfaces 2022; 28: 101649.

Yasim NSEM, Ismail ZS, Zaki SM, Azis MFA. Adsorption of Cu, As, Pb and Zn by banana trunk. Malaysian Journal of Analytical Sciences 2016; 20(1): 187-196.

Yu T, Chen Y, Zhang Y, Tan X, Xie T, Shao B, Huang X. Novel reusable sulfate-type zirconium alginate ion-exchanger for fluoride removal. Chinese Chemical Letters 2021; 32(11): 3410-3415.